Stanford Exploration Project, Report 111, June 9, 2002, pages 123–138

Stanford Exploration Project, Report 111, June 9, 2002, pages 123–138

Prestack imaging of overturned and prismatic reflections by reverse time migration

Biondo Biondi[1]

ABSTRACT

I present a simple method for computing angle-domain Common Image Gather (CIG) using prestack reverse time migration. The proposed method is an extension of the method proposed by Rickett and Sava (2001) to compute CIGs by downward-continuation shot-profile migration. I demonstrate with a synthetic example the use of the CIG gathers for migration velocity updating. A challenge for imaging both overturned and prismatic reflections is the discrimination of the reflection generated on either side of interfaces. I show how the propagation direction of the reflections can be easily determined by evaluating the crosscorrelation of the source wavefield with the receiver wavefield at time lags different than zero. Reflections can be easily separated once their direction of propagation is determined. I demonstrate the method by imaging overturned events generated by a segment of dipping reflector immersed in a vertically layered medium. The example shows that for overturned reflections velocity errors cause asymmetric residual moveouts. This observation suggests that for updating the velocity from overturned reflections, the migrated CIGs should be scanned using a different family of residual moveouts than the standard parabolic moveouts used for non-overturned events. The migration of a synthetic example containing prismatic reflection shows that the CIGs computed using only horizontal subsurface offset are not useful, and that the vertical subsurface offset should be also used.

INTRODUCTION

As seismic imaging is applied to more challenging situations where the overburden is ever more complex (e.g., imaging under complex and rugose salt bodies) and the illumination of important reflectors is spotty, we need to use all the events in the data to generate interpretable images. Two classes of events that are often neglected, but that are also often present in complex data are overturned reflections (Li et al., 1983) and prismatic reflections (Broto and Lailly, 2001). These two classes of events share the challenge that they cannot be imaged correctly (at least in laterally varying media) by downward-continuation migration methods. This obstacle prompted me to look at reverse time migration (Baysal et al., 1983), and in particular at reverse time migration of shot profiles (Etgen, 1986b).

[1]**email:** biondo@sep.stanford.edu

However, the current status of reverse-time migration technology has some limitations that need to be addressed before it can be used effectively to image either overturned or prismatic reflections. The main challenge is the extraction of useful and robust velocity updating information from the migrated image. In complex media, velocity is usually updated from the information provided by migrated Common Image Gathers (CIG). Filho (1992) presented the only other method that I am aware of to compute angle-domain CIGs (ADCIGs) by reverse time migration. He applied the method to Amplitude Versus Angle (AVA) analysis. His method is computationally involved and does not seem to be particularly robust because it requires the identification of local plane waves.

In this paper, I extend to reverse-time shot-profile migration the method that Rickett and Sava (2001) proposed to compute CIGs by downward-continuation shot-profile migration. The idea is to compute offset-domain CIGs by a modified imaging condition that introduces the concept of a *subsurface offset*. Simple testing using synthetic data confirmed that the CIG computed applying the proposed method can be used for velocity updating. They should also be useful for AVA analysis, though I have not yet analyzed their amplitude properties. However, for both overturned reflections and prismatic reflections, the source wavefield and the receiver wavefield may be propagating along opposite vertical directions at the reflection point. For these two classes of events, the imaging principle should be generalized to include a *vertical subsurface offset* as well an horizontal one. I have not tested this generalization of the CIG methodology yet.

The proper imaging of both overturned waves and prismatic reflections presents another challenge related to the discrimination between the image contributions of reflections generated from either side of an interface. These two reflections need to be discriminated both for imaging of reflectivity and for robust velocity updating, because these two reflections have usually opposite polarity, and their kinematics are affected by different areas of the velocity model. I present a simple generalization of the imaging condition that enables the determination of the propagation direction of the reflections, and thus the separation of the image contributions related to different events.

Reverse time migration has some other known disadvantages that need to be addressed. One of them is the computational cost. A companion short note in this report (Biondi, 2002) is an attempt to address this issue, at least for 3-D marine data. The artifacts caused by discontinuities in the migration velocity model are a more fundamental problem. There are a number of proposed solutions in the literature (Baysal et al., 1984; Etgen, 1986a; Filho, 1992). None of them is completely satisfactory, and thus more research on the subject is needed.

ANGLE-DOMAIN COMMON-IMAGE GATHERS BY REVERSE TIME MIGRATION

The standard imaging condition for prestack reverse time migration is based on the crosscorrelation in time of the source wavefield (S) with the receiver wavefield (R). The equivalent of the stacked image is the average over the sources (s) of the zero lag of this crosscorrelation,

that is:

$$I(z,\mathbf{x}) = \sum_s \sum_t S_s(t,z,\mathbf{x})\, R_s(t,z,\mathbf{x}), \tag{1}$$

where z and $\mathbf{x}$ are respectively depth and the horizontal axes, and t is time. The image created using this imaging condition is the equivalent to the stack over offsets for Kirchhoff migration.

This imaging condition has the disadvantage of not allowing a prestack analysis of the image for either velocity updating or amplitude analysis. The conventional way of overcoming this limitation is to avoid the averaging over sources, and thus to create CIGs where the horizontal axis is related to a *surface offset*; that is, the distance between the source location and the image point. This kind of CIG is known to be prone to artifacts even when the migration velocity is correct because the non-specular reflections do not destructively interfere. Furthermore, in presence of migration velocity errors and structural dips, this kind of CIG does not provide useful information for improving the velocity function.

Rickett and Sava (2001) proposed a method for creating more useful angle-domain CIGs with shot profile migration using downward continuation. Their method can be easily extended to reverse time migration. Equation (1) can be generalized by crosscorrelating the wavefields shifted with respect to each other. The prestack image becomes function of the horizontal relative shift, that has the physical meaning of a *subsurface offset* ($\mathbf{x}_h$). It can be computed as

$$I(z,\mathbf{x},\mathbf{x}_h) = \sum_s \sum_t S_s\left(t,z,\mathbf{x}+\frac{\mathbf{x}_h}{2}\right) R_s\left(t,z,\mathbf{x}-\frac{\mathbf{x}_h}{2}\right) \tag{2}$$

This imaging condition generates CIGs in the offset domain that can be easily transformed to the more useful ADCIG applying the same methodology described in (Sava et al., 2001).

Reverse time migration is more general than downward continuation migration because it allows events to propagate both upward and downward. Therefore the ADCIG computed from reverse time migration can be more general than the ones computed from downward-continuation migration. This more general imaging condition is actually needed when the source and receiver wavefields meet at the reflector when propagating along opposite vertical direction. This condition may occur either when we image overturned events or image prismatic reflections. I analyze these situations in more details in the following sections. To create useful ADCIGs in these situations we can introduce a *vertical offset* z_h into equation (2) and obtain

$$I(z,\mathbf{x},z_h,\mathbf{x}_h) = \sum_s \sum_t S_s\left(t,z+\frac{z_h}{2},\mathbf{x}+\frac{\mathbf{x}_h}{2}\right) R_s\left(t,z-\frac{z_h}{2},\mathbf{x}-\frac{\mathbf{x}_h}{2}\right) \tag{3}$$

These offset-domain CIGs should be amenable to being transformed into angle-domain CIG, by generalizing the methodology described in (Sava et al., 2001). However, I have not tested it yet, and in the examples I show only the application of the less general equation (2).

Examples of ADCIG to a simple synthetic data set

To illustrate the use of the proposed method to compute ADCIG I created a simple synthetic data set using a pseudo-spectral modeling code and then migrated the recorded shots using the

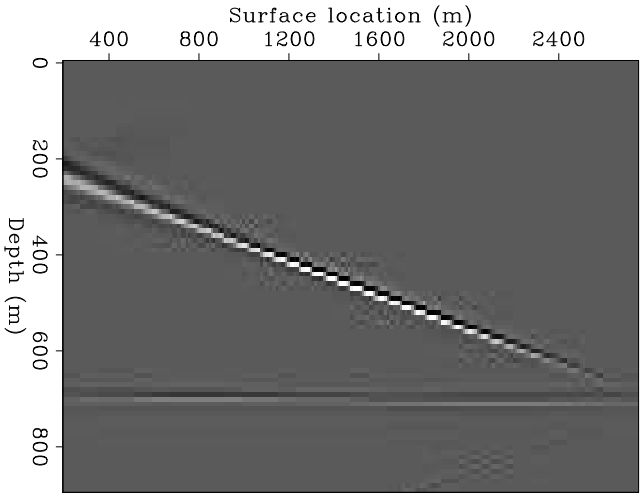

Figure 1: Image of the synthetic data set with the correct velocity function. biondo2-Shot-Image-dip [CR]

same pseudo-spectral wave-propagation kernel.

I modeled and migrated 100 shots spaced 10 m apart, starting from the surface coordinate of 1,000 m. The receivers were in a symmetric split-spread configuration with maximum offset of 2,550 m. I assumed two reflectors: one dipping 10 degrees and the other flat. The dipping reflector is shallower than the flat one. To avoid artifacts caused by velocity discontinuities in the migration velocity the reflectors were modeled as thin high-velocity (1.5 km/s) layers in a constant velocity medium (1 km/s). The migration velocity was set to constant, and equal to the background velocity. Therefore, the deeper reflector is slightly undermigrated.

Figure 1 is the image obtained applying the conventional imaging principle [equation (1)]. The dipping reflector is properly imaged within the range that is illuminated by the shots. The flat reflector is slightly undermigrated, as mentioned above.

Figure 2 shows on the left the offset-domain CIG (a) and on the right the angle-domain CIG (b). The CIGs are located at a surface location where both reflectors are illuminated well (1,410 m). As expected, the image is nicely focused at zero-offset in the panel on the left and the events are flat in the panel on the right.

To illustrate the usefulness for velocity updating of the proposed method to compute AD-CIGs, I have migrated the same data set with a lower velocity (.909 km/s). Figure 3 is the "stacked" image obtained using the lower velocity. Both reflectors are undermigrated and shifted upward.

Figure 4 shows on the left the offset-domain CIG (a) and on the right the angle-domain CIG (b). Now in the panel on the left, the energy is not focused at zero offset, but it is spread over an hyperbolic trajectory centered at zero offset. The corresponding ADCIG (right) shows the characteristic smile typical of an undermigrated ADCIG. The velocity information contained in the panel on the right can be easily used for velocity updating and tomographic inversion in a similar way as the ADCIG obtained by downward-continuation migrations are used (Clapp and Biondi, 2000; Clapp, 2001).

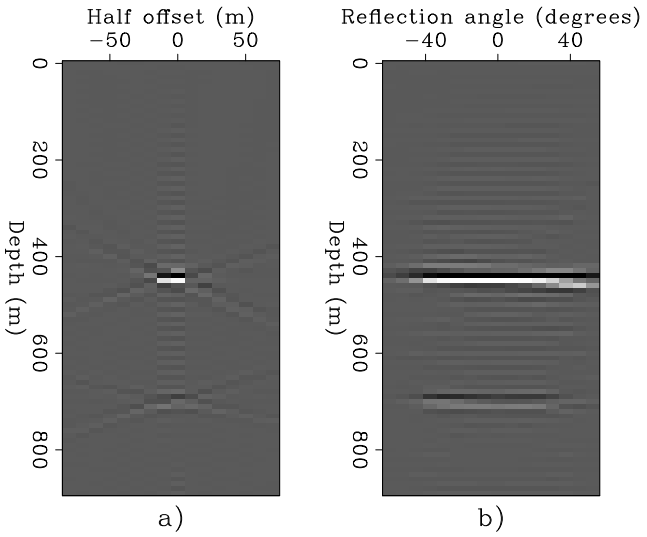

Figure 2: Offset-domain CIG (left a)) and angle-domain CIG (right b)) corresponding to the image in Figure 1. Notice the focusing at zero offset in a), and the flatness of the moveout in b). biondo2-Shot-Cig-Ang-dip [CR]

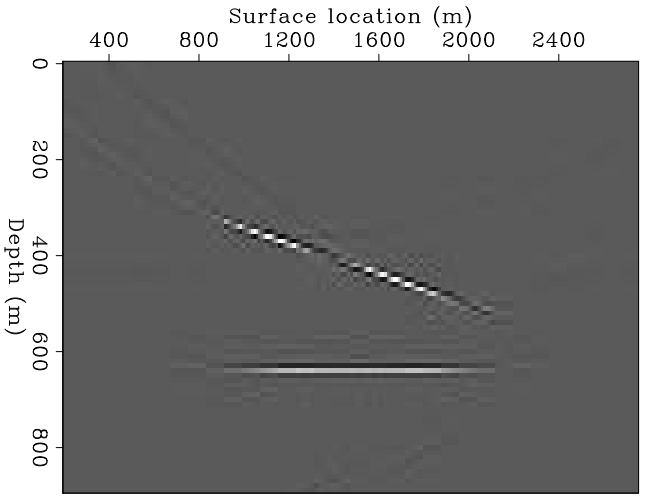

Figure 3: Image of the synthetic data set with the incorrect velocity function. biondo2-Shot-Image-dip-slow [CR]

PRESTACK IMAGES OF OVERTURNED REFLECTIONS

One of the main advantages of reverse-time migration methods over downward-continuation migration methods is their capability of imaging overturned events, even in presence of lateral velocity variations. However, this potential has not been exploited yet for prestack migration for several reasons. The computational cost is an important obstacle that is slowly being removed by progress in computer technology. In this section I will address two more fundamental problems. First, discrimination between image contributions from reflections generated above an interface from the image contributions from reflections generated below the same interface. These two reflections have usually opposite polarities because they see the same impedance contrast from opposite directions. If their contributions to the image are simply stacked together, they would tend to attenuate each other. Second, the updating of the migration velocity from overturned reflections. Solving the first problem is crucial to the solution of the second one, as graphically illustrated in Figure 5. This figure shows the raypaths for both events. It is evident that the overturned event passes through an area of the velocity field

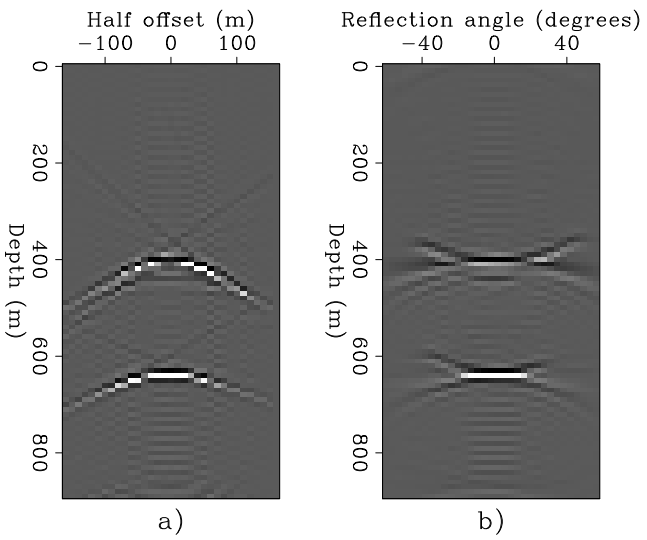

Figure 4: Offset-domain CIG (left) and angle-domain CIG (right) corresponding to the image in Figure 3. Notice the lack of focusing at zero offset in a), and the smile in b). biondo2-Shot-Cig-Ang-dip-slow [CR]

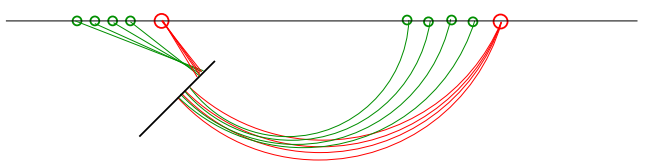

Figure 5: Ray paths corresponding to the reflection generated above the reflector and the one generated below the reflector. The rays corresponding to the source wavefield are red (dark in B&W), lines represent the wavefronts and the rays corresponding to the receiver wavefield are green. (light in B&W), biondo2-imag-rays [NR]

different from the area traversed by the reflection from above. The information on the required velocity corrections, provided by the image obtained using a given velocity function, can thus be inconsistent for the two reflections, even showing errors with opposite signs.

The reflection from above and the reflection from below can be discriminated by a simple generalization of the imaging principle expressed in equation (2), that includes a time lag τ in the crosscorrelation. To understand this generalization it is useful to review the process of image formation in reverse time migration. Figures 6–8 sketches this process at three different values in the propagation time t. For simplicity, the sketches represent the process for the familiar reflection from above, but similar considerations would hold also for the reflection from below. The reddish (dark in B&W) lines represent the wavefronts for the source wavefield. The greenish (light in B&W) lines represent the wavefronts for the receiver wavefield. At time $t - dt$ (Figure 6) the two wavefronts do not intersect, and thus they do not contribute to the crosscorrelation. At time t (Figure 7) the two wavefronts begin to interfere, and thus they begin to contribute to the image. The contribution starts in the middle of the reflector at time t, and then it moves to the sides as the time progresses to $t + dt$ (Figure 8). The process described above correlates the wavefields at the same time $(t - dt, t, t + dt)$. However, the wavefields can also be correlated at a non-zero lag over the time axis. In mathematical terms,

we can generalize equation (2) as

$$I(z,x,h,\tau) = \sum_t S\left(t+\frac{\tau}{2},z,x+\frac{h}{2}\right) R\left(t-\frac{\tau}{2},z,x-\frac{h}{2}\right). \tag{4}$$

Now the image is function of an additional variable τ, that represents the correlation lag in time. Figures 9–10 provide an intuitive understanding of the outcome of the correlation for $\tau = -dt/2$ (Figure 9) and $\tau = dt/2$ (Figure 10). In both cases the two wavefields interfere and they contribute to the image. For negative τ the image is slightly above the correct location of the reflector, and for positive τ the image is slightly below it. Therefore, the image of the reflector slowly moves downward (more precisely along the normal to the reflector) as τ increases. The crucial point is that for reflections generated from below, this movement is in the opposite direction (i.e., upward). This difference in propagation direction allows an easy discrimination of the two reflections by filtering the image according to the propagation direction as τ progresses. I have not implemented such a filtering yet, but it should be relatively straightforward.

I have confirmed this intuitive understanding by applying the generalized imaging condition in equation (4) to both the synthetic data set described above, and a synthetic data set with overturned events. I describe the results of the test on the latter in the next section.

Examples of prestack imaging of overturned reflections

To illustrate the use of the proposed method to image overturned reflections I created a simple synthetic data set that contains such events. I immersed a thin high-velocity segment in a layered medium with a strong vertical velocity gradient ($.97s^{-1}$). The reflector is dipping 44 degrees with respect to the vertical and extends from a surface coordinate of 1 km to a surface coordinate of 1.35 km.

I modeled and migrated 20 shots spaced 50 m apart, starting from the surface coordinate of 4.5 km. The receivers were in a symmetric split-spread configuration with maximum offset of 6.4 km. Because of the relative position of the reflector with respect to the shots, only the overturned reflections illuminate the reflector.

Figure 11 is the image obtained by applying the conventional imaging principle; that is; evaluating equation (4) at $\tau = 0$. The dark segment superimposed onto the image shows the position of the reflector in the model. The reflector is properly focused and positioned correctly. Figure 12 shows the image at $\tau = -.00525s$ (top) and the image at $\tau = .00525s$ (bottom). As in Figure 11, the dark segment superimposed onto the images shows the position of the reflector in the model. In these two panels the reflector is almost as well focused as in Figure 11, but it is slightly shifted along its normal. As expected from the theoretical discussion above, the reflector is slightly lower for the negative τ (top) than for the positive τ (bottom).

Figure 13 shows an example of CIG computed by evaluating equation (4) at $\tau = 0$. The panel on the left (a) shows the offset-domain CIG, and the panel on the right (b) shows the

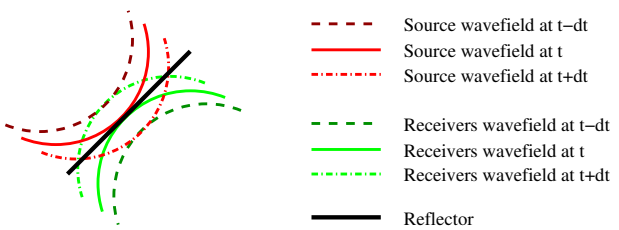

Figure 6: Wavefronts for the source wavefield (red), and the receiver wavefield (green), for three time steps $(t-dt, t, t+dt)$. The wavefronts at $t-dt$ are highlighted in darker color. The two highlighted wavefronts do not intersect, and thus their contribution to the image is null. biondo2-image-wave-st-m1 [NR]

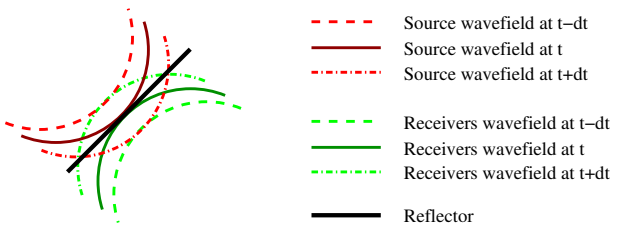

Figure 7: Wavefronts as in Figure 6. The two highlighted wavefronts (time t) intersect in the middle of the reflector, and they contribute to the image at the intersecting point. biondo2-image-wave-st-0 [NR]

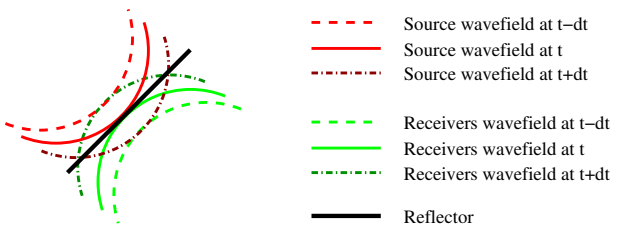

Figure 8: Wavefronts as in Figure 6. The two highlighted wavefronts (time $t+dt$) intersect at the edges of the reflector, and they contribute to the image at the intersecting points. biondo2-image-wave-st-p1 [NR]

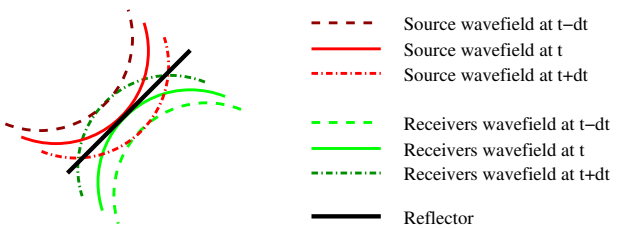

Figure 9: Wavefronts as in Figure 6. The two highlighted wavefronts (source wavefront at time $t-dt$ and the receiver wavefront at time $t+dt$) intersect above the reflector, and they contribute to the image at the intersecting point. biondo2-image-wave-lag-m1 [NR]

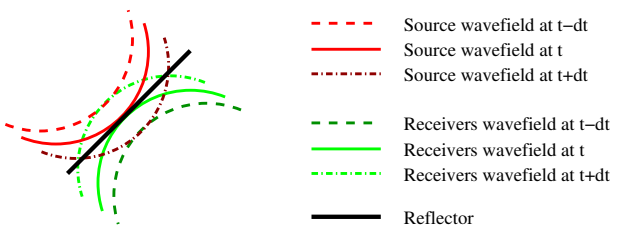

Figure 10: Wavefronts as in Figure 6. The two highlighted wavefronts (source wavefront at time $t+dt$ and the receiver wavefront at time $t-dt$) intersect below the reflector, and they contribute to the image at the intersecting point. biondo2-image-wave-lag-p1 [NR]

angle-domain CIG. The energy is correctly focused at zero offset in a), and the event is flat in b), though the angular coverage is narrow because of the short range of shot locations (1 km).

The second obstacle to image overturned reflections is the estimation of a velocity model that focuses and positions them correctly. To investigate this issue, I migrated the same data set with two inaccurate velocity functions. The first is 1% slower than the correct one, and the second is 1% faster than the correct one. Figure 14 shows the "stacked" images produced by these two migrations. The panel on the top (a) shows the image when the velocity is too low, and the panel on the bottom (b) shows the image when the velocity is too high. As in the previous figures, the dark segment superimposed onto the images shows the position of the reflector in the model. As expected the reflector is mispositioned and not as well focused as in Figure 11.

Figure 15 shows the CIG gathers taken at the same location as in Figure 13 for the migration with the low velocity and Figure 15 shows the CIG gathers for the migration with the high velocity. Notice that the velocity errors have caused a shift along the offset direction of the focal point in the offset-domain gathers. Towards positive offsets for the low velocity (Figure 15) and towards negative offsets for the high velocity (Figure 16). The angular coverage is too limited to notice a clear pattern in the angle-domain CIGs. In principle, a lateral shift in offset-domain gather should correspond to a tilt in the angle-domain gathers. These results seems to indicate that the residual moveout is asymmetric for overturned reflections, contrary to the symmetric moveout caused by velocity errors for regular reflections (see Figure 4). A more definitive analysis requires the migration of a survey with wider angular coverage; that is, with wider shot range. However, this characteristic suggests that for updating the velocity from overturned waves, the migrated CIGs should be scanned using a different family of residual moveouts than the parabolic moveouts used for standard reflections. The shift in the focal point in the offset-domain gathers could be also directly used for updating the velocity along the path of the overturned reflections.

PRESTACK IMAGES OF PRISMATIC REFLECTIONS

Prismatic reflections are another class of reflections that can be potentially useful for imaging complex data. They usually include at least a segment of the ray path that is propagating upward. Therefore, downward continuation method are not appropriate for imaging them.

To test the possibility of using reverse time migration to image prismatic reflection I created another synthetic data set. Figure 17 shows the velocity model used for generating the synthetic. The solid line superimposed onto the velocity is an example of prismatic-reflection ray path. I modeled and migrated 250 shots spaced 6.25 m apart, starting from the surface coordinate of 1,375 m. The receivers were in a symmetric split-spread configuration with maximum offset of 6,400 m.

To better analyze the behavior of reverse time migration in imaging prismatic reflections, I removed the primary reflections from the data. To achieve this goal I subtracted two other

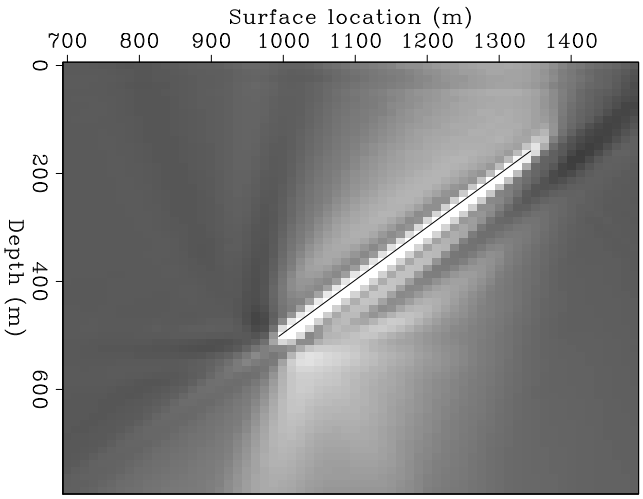

Figure 11: Image of the synthetic data set containing the overturned reflections migrated with the correct velocity and at $\tau = 0$. The dark segment superimposed onto the images shows the position of the reflector in the model. biondo2-Shot-Refl-Image-vover [CR]

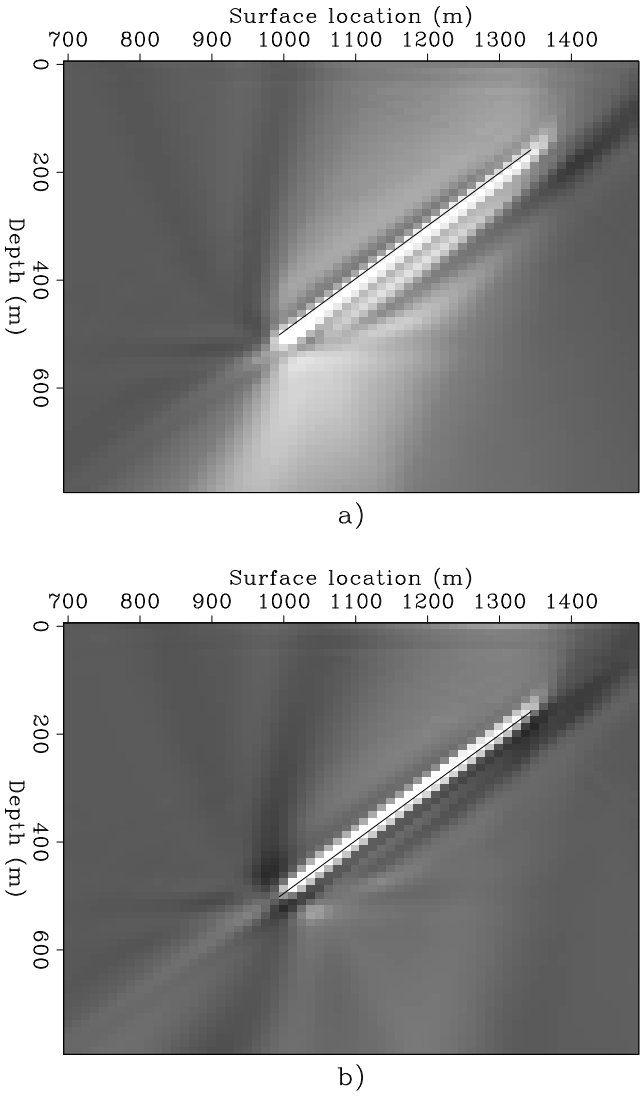

Figure 12: Images of the synthetic data set containing the overturned reflections migrated with the correct velocity; at $\tau = -dt/2$ (top) and at $\tau = dt/2$ (bottom) The dark segment superimposed onto the images shows the position of the reflector in the model. Notice the slight downward shift of the imaged reflector in a) and the slight upward shift of the imaged reflector in b). biondo2-Shot-Refl-Image-mov-vover [CR]

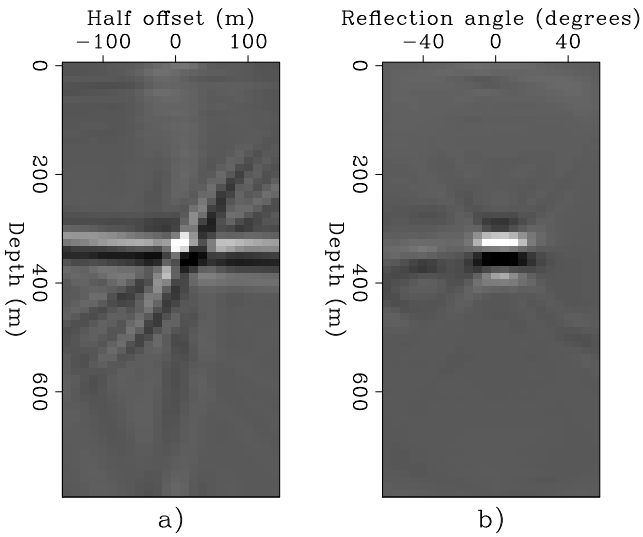

Figure 13: Offset-domain CIG (left) and angle-domain CIG (right) corresponding to the image in Figure 11. Notice the focusing at zero offset in a), and the flatness of the moveout in b), though the angular coverage is narrow because of the short range of shot locations (1 km). biondo2-Shot-Cig-Ang-vover [CR]

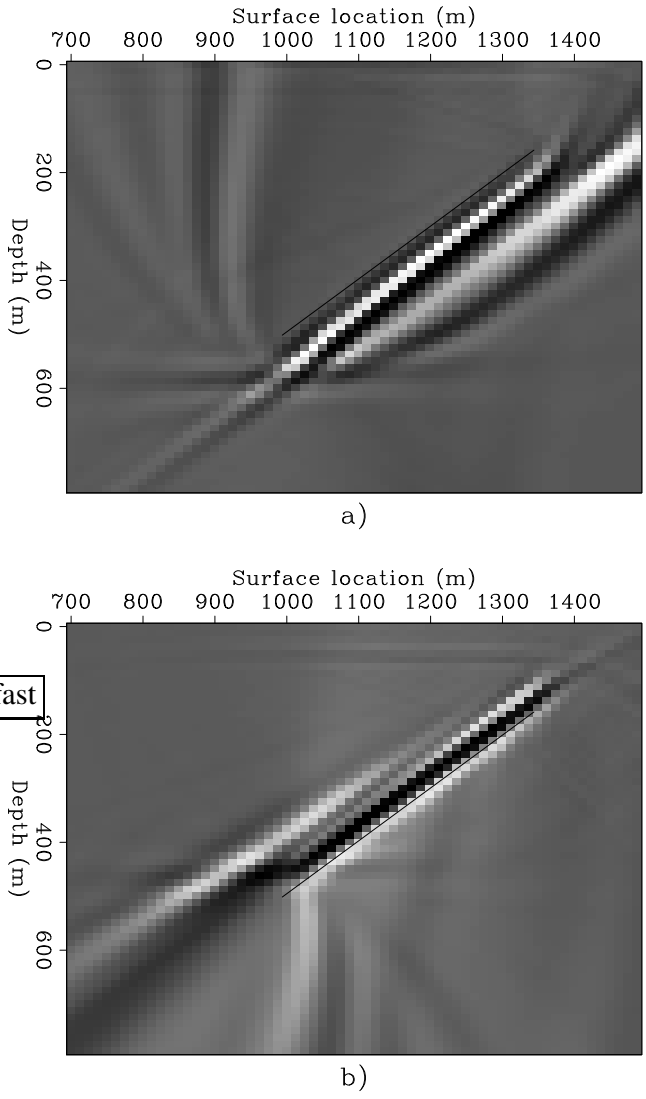

Figure 14: Image of the synthetic data set containing the overturned reflections migrated with a velocity function 1% lower than the correct one (top) and with a velocity function 1% higher than the correct one (bottom). Notice the misfocusing and mispositioning of the reflector. biondo2-Shot-Refl-Image-vover-slow-fast [CR]

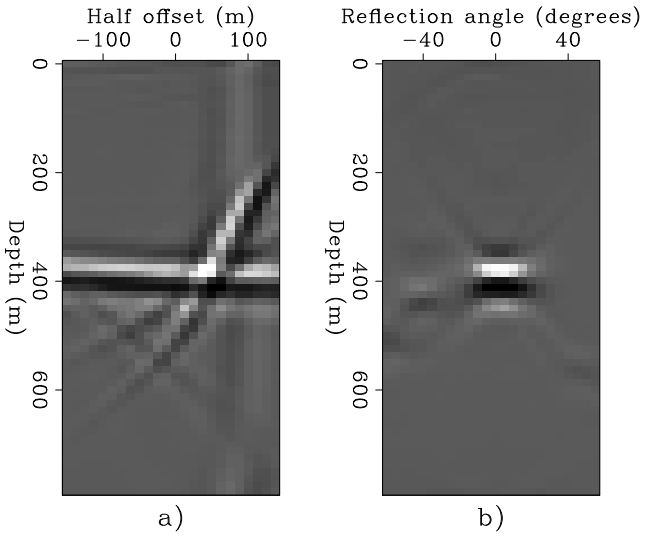

Figure 15: Offset-domain CIG (left) and angle-domain CIG (right) corresponding to the image in Figure 14a. Notice the positive shift along the offset direction of the focal point in the offset-domain gathers. biondo2-Shot-Cig-Ang-vover-slow [CR]

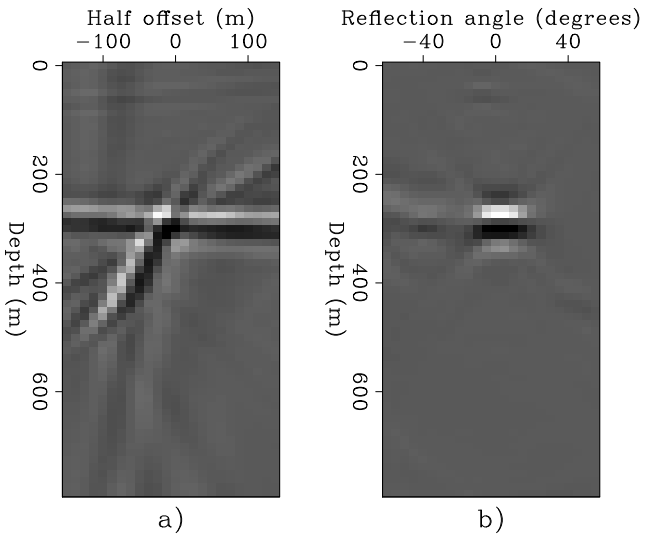

Figure 16: Offset-domain CIG (left) and angle-domain CIG (right) corresponding to the image in Figure 14b. Notice the negative shift along the offset direction of the focal point in the offset-domain gathers. biondo2-Shot-Cig-Ang-vover-fast [CR]

data sets from the data modeled assuming the velocity model shown in Figure 17. One of the data sets included the primary reflections from the flat reflector, and the other one the primaries from the dipping reflector. The two velocity models used to generate the primaries were created by breaking the black area shown in Figure 17 into two pieces, divided by a vertical line passing through the location of the corner (1.4 km).

To image prismatic reflections, the background velocity function needs to include at least one of the interfaces that generated the reflections. I assumed that the flat reflector was known, and thus I included a flat velocity interface at 600 m depth in the migration velocity model. Figure 18 is the image obtained migrating all the 250 shots. As expected by simple analysis of the raypaths, the prismatic reflections illuminate the dipping reflector more strongly in the deeper part than in the shallower part. The image shows also a high energy flat event on the right side of the corner, that is not a proper image of a reflection. In theory, such event should not be there. The primaries associated with the flat reflector were removed from the data. The prismatic reflections bouncing off the dipping layer are not imaged because the dipping layer is not present in the migration velocity. This artifact is likely to be caused by the (imperfect) correlation of the prismatic reflection (solid line in Figure 17) with reflections generated by the horizontal discontinuity in the migration velocity model (dashed line in Figure 17). This interpretation is corroborated by the presence of a faint low-frequency noise extending upward from the flat reflector.

Figure 19 shows on the left the offset-domain CIG (a) and on the right the angle-domain CIG (b). The CIGs are located at a surface location where prismatic reflections illuminate the dipping reflector (1,350 m). The energy focuses at zero offset, but the angle-domain CIG is not flat. This lack of flatness is likely to be caused by the fact that the source and receiver wavefields meet at the reflector when propagating along opposite vertical direction. I speculate that better angle-domain CIGs could be generated if I applied the generalized imaging condition expressed in equation (3), that includes the vertical subsurface offset.

CONCLUSIONS

I presented a method to compute Common Image Gathers from reverse-time shot profile migration. The proposed method generates accurate CIGs that can be used to update the migration velocity function, both for regular reflections and for overturned reflections.

The reflections generated from either side of an interface can be discriminated by computing the crosscorrelation of the source wavefield with the receiver wavefield at the non-zero time lag. This techniques is useful for imaging both overturned reflections and prismatic reflections.

The migration of a synthetic example containing prismatic reflections suggests that imaging this kind of reflections might be prone to artifacts and may require the computation of the CIGs with the even more general imaging condition that includes vertical subsurface offset.

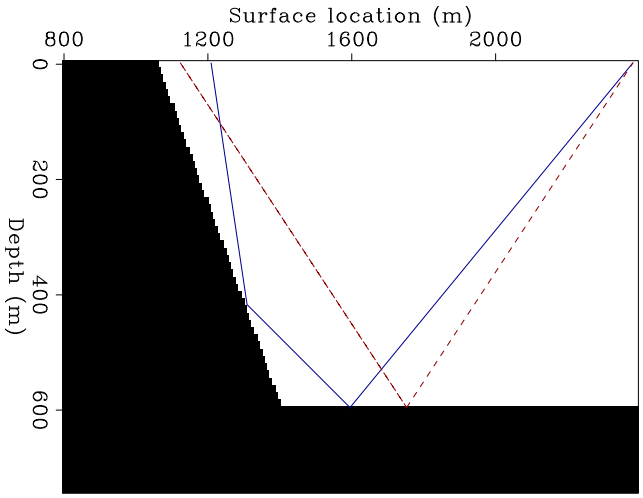

Figure 17: Velocity model assumed to create the synthetic data set. Superimposed onto the velocity is an example of prismatic-reflection ray path (solid line). biondo2-Slow-prism-ann [NR]

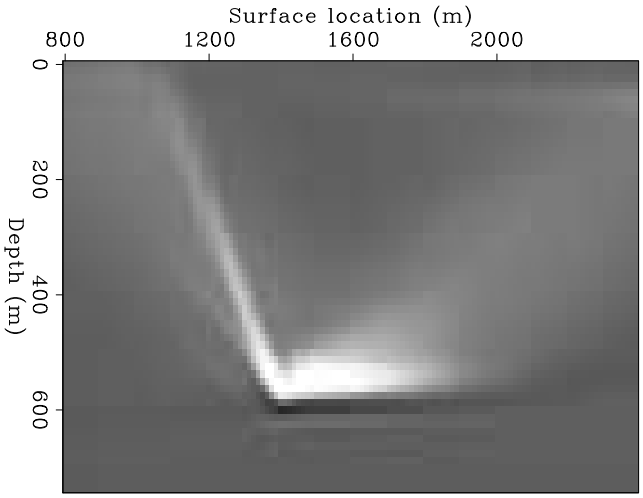

Figure 18: Image of the synthetic data set containing the overturned reflections migrated with the correct velocity and at $\tau = 0$. biondo2-Shot-Image-prism [CR]

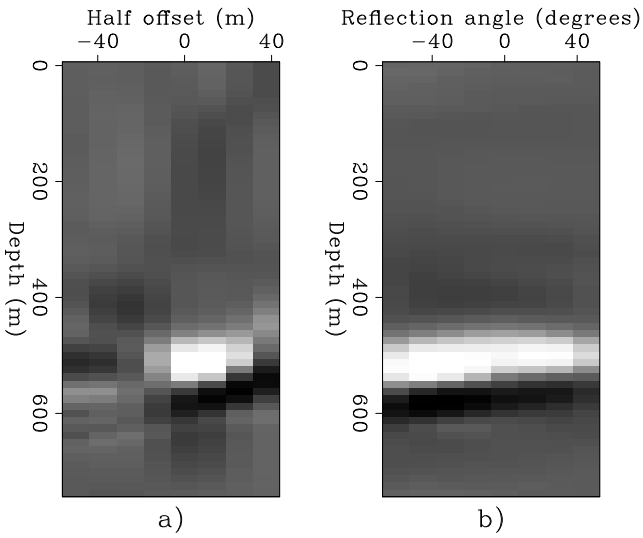

Figure 19: Offset-domain CIG (left) and angle-domain CIG (right) corresponding to the image in Figure 18. Notice that the energy focuses at zero offset, but that the angle-domain CIG is not flat. This lack of flatness is likely to be caused by the fact that the source and receiver wavefields meet at the reflector when propagating along opposite vertical direction. biondo2-Shot-Cig-Ang-prism [CR]

REFERENCES

Baysal, E., Kosloff, D. D., and Sherwood, J. W. C., 1983, Reverse time migration: Geophysics, **48**, no. 11, 1514–1524.

Baysal, E., Kosloff, D. D., and Sherwood, J. W. C., 1984, A two-way nonreflecting wave equation: Geophysics, **49**, no. 02, 132–141.

Biondi, B., 2002, Reverse time migration in midpoint-offset coordinates: SEP–**111**, 149–157.

Broto, K., and Lailly, P., 2001, Towards the tomographic inversion of prismatic reflections: 71st Ann. Internat. Mtg., Soc. Expl. Geophys., Expanded Abstracts, 726–729.

Clapp, R., and Biondi, B., 2000, Tau domain migration velocity analysis using angle CRP gathers and geologic constrains: 70th Ann. Internat. Mtg., Soc. of Expl. Geophys., Expanded Abstracts, 926–929.

Clapp, R. G., 2001, Geologically constrained migration velocity analysis: Ph.D. thesis, Stanford University.

Etgen, J., 1986a, High order finite-difference reverse time migration with the two way nonreflecting wave equation: SEP–**48**, 133–146.

Etgen, J., 1986b, Prestack reverse time migration of shot profiles: SEP–**50**, 151–170.

Filho, C. A. C., 1992, Elastic modeling and migration in earth models: Ph.D. thesis, Stanford University.

Li, Z., Claerbout, J. F., and Ottolini, R., 1983, Overturned-wave migration by two-way extrapolation: SEP–**38**, 141–150.

Rickett, J., and Sava, P., 2001, Offset and angle domain common-image gathers for shot-profile migration: 71st Ann. Internat. Meeting, Soc. Expl. Geophys., Expanded Abstracts, 1115–1118.

Sava, P., Biondi, B., and Fomel, S., 2001, Amplitude-preserved common image gathers by wave-equation migration: 71st Ann. Internat. Mtg., Soc. Expl. Geophys., Expanded Abstracts, 296–299.